Journal of Materials Chemistry A

Accepted Manuscript

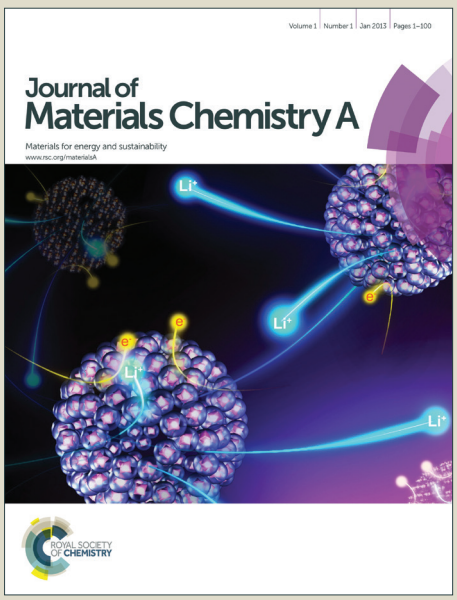

ROYAL SOCIETY OF CHEMISTRY

www.rsc.org/materialsA

The table of contents entry

Nanocups-on-Microtubes: a Unique Host Towards High-Performance Lithium Ion Batteries

Junhua Kong, Chenyang Zhao, Yuefan Wei, Si Lei Phua, Yuliang Dong, and Xuehong Lu*

Carbonaceous nanocups attached on free-standing microtubes were prepared and used to trap MoS_2 nanosheets. Excellent cyclability and rate performance was achieved owing to the efficient contact among nanocups, nanosheets and electrolyte.

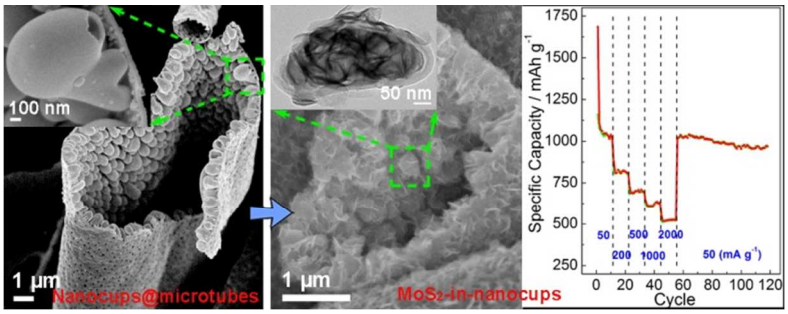

Cite this: DOI: 10.1039/c0xx00000x

www.rsc.org/xxxxxx

ARTICLE TYPE

Nanocups-on-Microtubes: a Unique Host Towards High-Performance Lithium Ion Batteries

Junhua Kong,[a,#] Chenyang Zhao,[a,#] Yuefan Wei,[b] Si Lei Phua,[a] Yuliang Dong,[a] and Xuehong Lu*[,a]

Received (in XXX, XXX) Xth XXXXXXXXX 20XX, Accepted Xth XXXXXXXXX 20XX

DOI: 10.1039/b000000x

In this work, unique carbonaceous nanocups densely attached on a free-standing hollow microfibrous mat were prepared via mussel-inspired biomimetic polydopamine (PDA) coating process using electrospun porous microfibers as the templates, followed by annealing. Electron microscopic studies show that the diameters and depths of the ellipsoid-shaped nanocups are in the range of a few hundred nanometers while they have small openings of less than 100 nm, allowing the cups acting as nano-chambers to host other functional materials as well as acting as nano-reactors for synthesis of embedded nanostructures. To demonstrate the functions of such unique hollow structure, the nanocups were used to host MoS_2 precursor and through hydrothermal treatment, MoS_2 nanosheets were effectively trapped in the nanocups. The MoS_2-in-nanocups were used as an anode in lithium ion batteries. Good cyclability and excellent rate capacity (around 520 mAh g^{-1} at 2 A g^{-1}) was achieved owing to the efficient charge transport provided by the good contact of the MoS_2 nanosheets with the conductive nanocups and surrounding electrolyte. The nanocups could also act as buffering chambers to effectively accommodate the volume expansion of MoS_2 during cycling.

Introduction

In recent years there has been a considerable rise in interests in hollow nanostructures owing to their unique properties. Hollow nanostructures have shown great advantages over other types of nanostructures in many aspects. For example, they may offer facile transport channels for surrounded media, such as various liquids and ions, as well as provide extremely large surface area as interfacial contact and reaction sites.[1-4] Hollow nanostructures can also be used to host/support other active components to form multi-functional nanohybrids.[5-11] The geometric arrangements of the other components may be constrained by the hollow host/supporter, while the features of both the host and guest are integrated to evoke unique functions. Both organic and inorganic materials have been used to fabricate hollow nanostructures of various geometries, mainly hollow nanospheres and nanofibers.[12-15] The potential applications of these hollow nanostructures have been demonstrated in a wide variety of areas such as gas sensing, energy storage/harvesting, catalysis, health and biomedicine.[3, 7, 10, 12, 16-17]

Besides the popular hollow nanospheres and hollow nanofibers, other forms of hollow nanostructures with more sophisticated geometries are also in great demand as high-performance functional materials yet the fabrication of such hollow nanostructures is challenging. A typical example is nanocontainers/nanocups. Polymeric nanocontainers have been fabricated for entrapment of small molecules, inhibitors and drugs.[18-21] Various inorganic (TiO_2, SiO_2, Au, Fe_2O_3, Pt) nanocups have also been prepared and used as photocatalyst, charge conductor, etc.[22-26] In addition, chemical vapor deposition and ion irradiation on anodized aluminum oxide template have been used to form carbon nanocups.[27] However, the difficulty in mass production is still a major obstacle for practical applications of nanocups. Moreover, fabrication of bulk structures attached with a high population of nanocups, which may be useful for a wide variety of applications, has not been realized.

It is well known that electrospinning is a facile technique for large-scale fabrication of polymer nanofibers/microfibers. The technique can also render the nanofibers/microfibers various porous morphology, including densely distributed surface nanopores, through carefully selecting solvents and controlling processing conditions.[28-31] We hypothesized that such nanoporous electrospun fibers may be used as templates for large-scale fabrication of nanocups via mussel-inspired biomimetic polydopamine (PDA) coating process. This biomimetic process may enable excellent replication of the surface features of the electrospun fibers by the PDA coating, which can then be converted to highly electrically conductive nitrogen-doped graphite-like thin coating through carbonization.[32] Since the electrospun fibers can be collected in the form of a free-standing mat, the approach may also allow the nanocups be attached on a bulk structure. This would facilitate their applications in various areas, e.g. the nanocups may be easily handled to act as nano-chambers to host other functional materials and/or they may act as nano-reactors for synthesis of embedded nanostructures. To verify the hypothesis and demonstrate that this is a unique platform for large-scale

fabrication of carbon nanocups supported on a bulk structure, in this work, we successfully fabricated carbon nanocups attached on hollow microfibers through self-polymerization of dopamine (DOPA) on electrospun porous fibers followed by annealing. To demonstrate their functions, the nanocups were used as nano-reactors to synthesize molybdenum disulfide (MoS_2) nanosheets, which have graphene-like layered structure and are promising anode material for lithium ion batteries (LIBs).[33-37] Electrochemical properties of the resultant hybrid mats were investigated. Good cyclability and excellent rate performance were achieved owing to the buffering effect provided by the nanocups and good contact of the thin MoS_2 nanosheets with the conductive nanocups and surrounding electrolyte.

Experimental

Materials

Polystyrene (PS, M_w = 350000), dopamine hydrochloride (DOPA), tris(hydroxymethyl) aminomethane (Tris), sodium molybdate dihydrate ($Na_2MoO_4{\cdot}2H_2O$) and thioacetamide (TAA, CH_3CSNH_2) were purchased from Sigma-Aldrich Chemistry (USA). Toluene and ethanol were supplied by Tedia Company Inc. (USA) and Merck KGaA (Germany), respectively.

Preparation of porous PS fibers

PS was dissolved in toluene under stirring at 60 °C. The solutions with 15 wt% and 25 wt% PS, respectively, were then electrospun into PS fibers under the following conditions: working voltage of 13 kV, feeding rate of 1.0 mL/h, and ethanol as liquid collector. For each solution, the PS fibers were collected for four hours using ethanol as the liquid collector and after the collection the PS fibers were suspended in ethanol for further use.

Preparation of nanocups-on-hollow microtubes

PDA was coated onto PS fibers via self-polymerization of DOPA as reported previously.[10] In brief, the suspended PS fibers were transferred into 490 g Tris aqueous solution (0.01 M). Polymerization was allowed for 2 hrs by adding 10 g DOPA aqueous solution (0.16 M) into PS-filled Tris solution under continuous shaking. The above process was conducted for another 5 times using freshly prepared Tris and DOPA solution to achieve enough PDA coating thickness. After drying at 60 °C under vacuum, the PDA-coated PS fibers were heated up to 700 °C at the heating rate of 5 °C/min and then kept at 700 °C for another 3 hrs in argon atmosphere. The product obtained was denoted as C-PDA nanocups.

Formation of MoS_2 nanosheets in C-PDA nanocups

MoS_2 was hydrothermally grown in the C-PDA nanocups using TAA and $Na_2MoO_4{\cdot}2H_2O$ as the precursors. A free-standing mat with C-PDA nanocups was vertically immersed into an aqueous solution of TAA (0.13 M) and $Na_2MoO_4{\cdot}2H_2O$ (0.06 M) for 6 hrs. It was then taken out and kept still for 0.5 hr. The C-PDA nanocups filled with the precursors were put into an empty glass bottle vertically, which was then transferred into a Teflon-lined stainless steel autoclave with filled DI H_2O. The hydrothermal growth was carried out at 200 °C for 24 hrs. The obtained sample was dried at 60 °C under vacuum and denoted as MoS_2-in-C-PDA nanocups.

Characterization

The morphology of the samples was investigated using a field-emission scanning electron microscope (FESEM, JEOL-7600F) and a transmission electron microscope (TEM, JEOL-2100). The specific surface area and pore size of the samples was measured using a surface area and porosity test system (Micromeritics, Tristar II 3020) after degassing at 140 °C in N_2 for overnight. The composition of the samples was measured using a thermogravimetric analyzer (TGA, Q500). The structure of the samples was studied using an X-ray diffractometer (XRD, Bruker D8 Discover GADDS).

Electrochemical measurements

The C-PDA nanocups and MoS_2-in-C-PDA nanocups were tested as anodes in LIBs. The battery assembly process and the electrochemical testing procedures were the same as that reported in a previous publication.[38] In brief, the C-PDA nanocups and MoS_2-in-C-PDA nanocups, which were in the form of free-standing mats, were used as anodes directly without binder and additive. The mats were in circular disc shape with diameter of 10 mm and weight of about 2 mg (mass loading: ~2.55 mg/cm^2). Lithium foil with thickness and diameter of 0.6 mm and 14 mm, respectively, and 1 M $LiPF_6$ in the mixture of ethylene carbonate and dimethyl carbonate with 1/1 volumetric ratio were used as the counter electrode and electrolyte, respectively. The anode and counter electrode were isolated by Celgard 2325 separator. All were assembled into 2032 cells in an argon-filled glove box with moisture and oxygen level less than 0.1 ppm. The assembled cells were connected to a battery test system (4200, MACCOR) for electrochemical performance evaluation. The voltage ranges from 3.0 V to 0.005 V for cycling and rate capacity measurements. The cyclic voltammetry (CV) test was performed at 0.1 mV/s within 3.0-0.005 V using an electrochemical workstation (PGSTAT302, Autolab).

Results and Discussion

Preparation of C-PDA nanocups and their morphologies

Polystyrene (PS) fibers were firstly prepared via conventional electrospinning using a liquid collector.[10] However, ethanol, instead of water, was used as the collection medium. When PS fibers hit the ethanol surface, they can quickly precipitate into ethanol owing to the relatively good wetting of the fiber surface by ethanol as well as large density difference between PS and ethanol. The timely precipitation of the electrospun PS fibers into ethanol prevents accumulation of the PS fibers on the liquid surface, preserving the conductive liquid surface for smooth electrospinning. The precipitated PS fibers form a loose lump in ethanol (Fig. 1a), providing large inter-fiber spaces to ensure uniform post-coating.[11] The field-emission scanning electron microscope (FESEM) images in Fig. 1b_1-1b_3 show the morphology of the PS fibers produced from the PS/toluene solution with 25 wt% PS. The PS fibers obtained are continuous long fibers with diameters of several micrometers. From the high-magnification images it can be clearly seen that a large quantity of pores are homogeneously created on the surface of the fibers and the average size of the pore openings is mainly less than 100 nm. The transmission electron microscope (TEM) side view

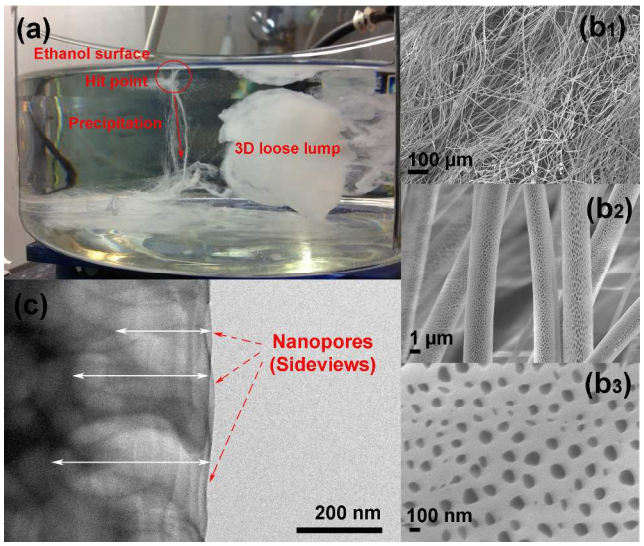

Fig. 1 (a) The collection of the PS fibers using ethanol. (b_1-b_3) FESEM and (c) TEM images of the as-prepared PS fibers, showing the highly porous morphology of the surface

image (Fig. 1c) of the edge of a single fiber reveals that the pores have irregular ellipsoid shape with the depths of a few hundred nanometers. Phase separation as well as breath figures is believed to be the main causes for the formation of such pores while solvent type and environmental humidity also play crucial roles.[28-31]

Since PS is able to fully decompose at temperatures slightly above 400 °C in inert environment, the porous PS fibers can be used as self-sacrificing templates to produce nanocups attached on hollow fibers in mass. The preparation process is illustrated in Fig. 2a. Due to the strong affinity of PDA to most solid surfaces,[39] DOPA molecules self-polymerize on the surface of the porous PS fibers, forming PDA coating that takes the shape of the porous fibers. The successful coating was verified by FESEM and TEM images (Fig. S1). Upon annealing, PS was removed while the PDA coating was converted to carbonized PDA (C-PDA) nanocups. Our previous studies[32] have shown that the C-PDA thin coatings obtained on flat substrates have graphitic layered structure with (002) *d* spacing and grain size of 0.41 and 5.3 nm, respectively, and their in-plane and trough-plane electrical conductivities are comparable to that of multi-layered graphene. Different from graphene, the C-PDA contains 7.1 % of oxygen and 4.5 % of nitrogen (N) as heteroatoms, as confirmed by X-ray photoelectron spectroscopy (XPS) analysis, and there are high percentages of pyridinic (35.2 %) and pyrrolic (52.4%) N.[32] These increase the structural disorder and distortion of the C-PDA, and favour reversible lithium adsorption. It is believed that the structure of the C-PDA nanocups should resemble that of the C-PDA thin coatings obtained on flat substrates because they were fabricated under the same polymerization and annealing conditions. The aforementioned structural features may hence render the C-PDA nanocups distinctly different electrochemical behavior/performance from other carbon allotropes, which will be elaborated later. As shown in Fig. $2b_1$-$2b_3$, the fibrous morphology with homogeneously distributed pore openings on

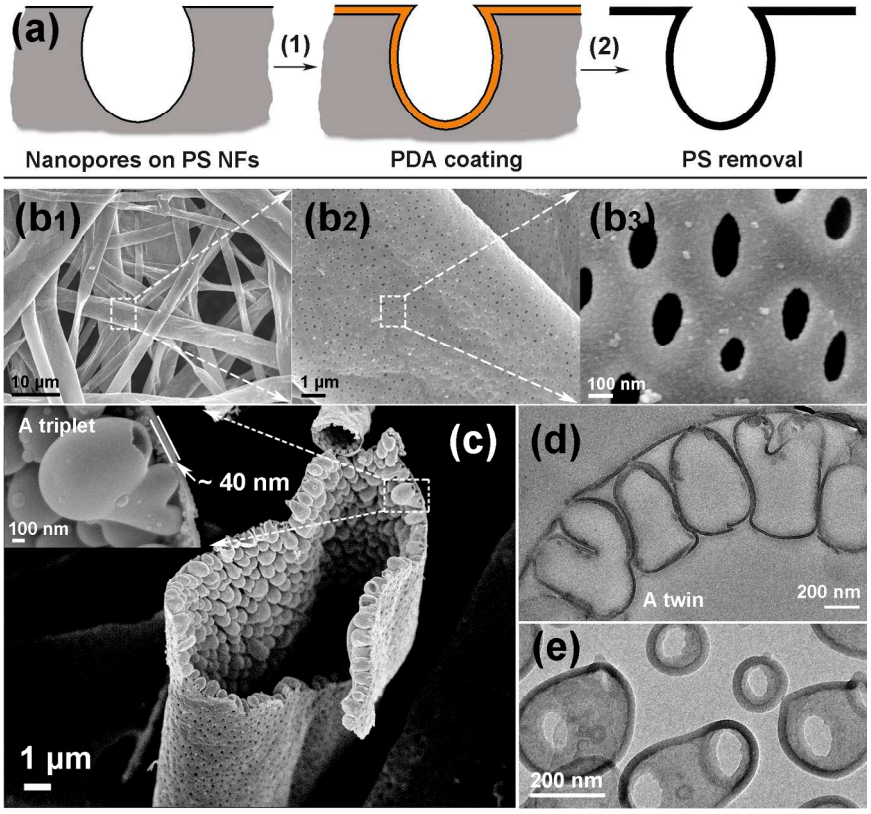

Fig. 2 (a) A scheme to show the formation of the C-PDA nanocups. (b_1-b_3) FESEM images of the fibers after removing PS. (c) Cross-sectional view of the C-PDA nanocups by FESEM; the inset shows a triplet of nanocups. (d) Cross-sectional view and (e) top view of the C-PDA nanocups by TEM

Cite this: DOI: 10.1039/c0xx00000x

www.rsc.org/xxxxxx

ARTICLE TYPE

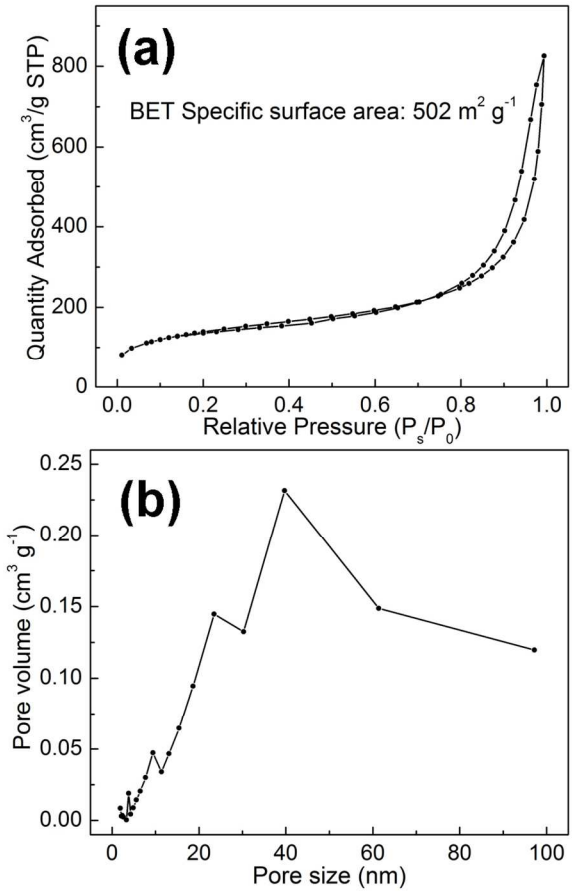

Fig. 3 (a) Brunauer-Emmett-Teller (BET) isotherm curve and (b) Barrett-Joyner-Halenda desorption pore size distribution of the C-PDA nanocups-on-microtubes

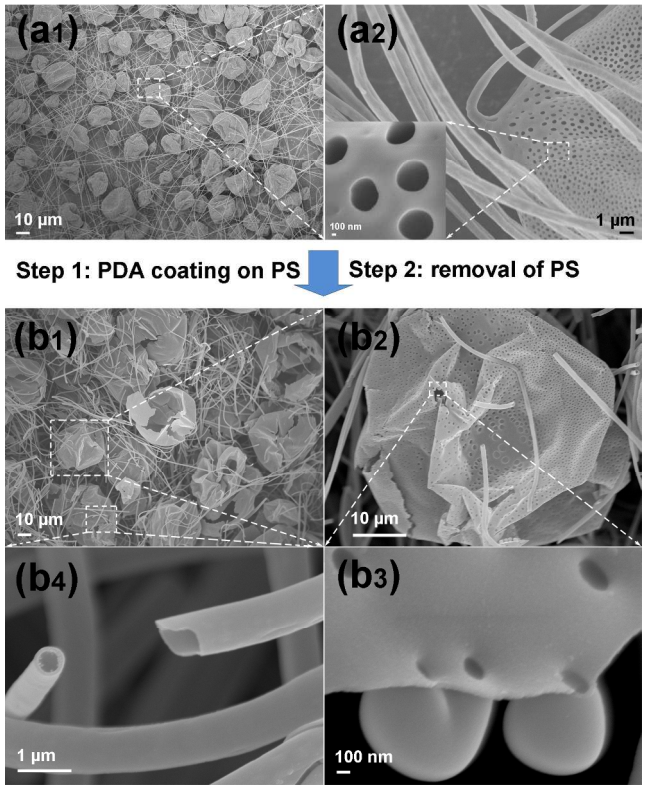

Fig. 4 SEM images showing the morphologies of (a_1-a_2) electrospinning-derived PS microbeads with surface nanopores, which are linked by nanofibers, as well as (b_1 - b_4) the corresponding hollow carbon structures obtained by annealing of PDA-coated PS microbeads

the surface is perfectly retained after annealing. As the PDA coating could replicate the surface of the porous PS fibers excellently, a large number of ellipsoid-shaped nanopores with small openings, which are denoted as nanocups in this work, are formed. As verified by FESEM studies (Fig. 2c), the nanocups are firmly attached on the C-PDA microtubes, which has the thickness of around 40 nm (inset of Fig. 2c). The FESEM (inset in Fig. 2c) and cross-sectional TEM images in Fig. 2d also show that the nanocups with dimension of a few hundred nanometers exist as either individual ellipsoid-shaped cup or inter-connected twins/triplets. This is also observed in the TEM top view image in Fig. 2e, where one chamber has one or two openings. The formation of single/twin/triplet nanocups implies that the nanopores on the surface of the electrospun PS fibers are randomly distributed and hence some nanopores are interpenetrating.

The attachment of nanocups onto microtubes provides much larger specific surface area than conventional hollow nanofibers with similar dimensions (Fig. S2a). As shown in Fig. 3, typical type IV N_2 absorption/desorption behavior is observed for the nanocups-on-microtubes, indicating the mesoporous feature of the nanostructure. The BET specific surface area is 502 m^2 g^{-1}, which is much higher than that of electrospinning-derived C-PDA hollow nanofibers (326 m^2 g^{-1}, Fig. S2b). The Barrett-Joyner-Halenda (BJH) desorption pore size of the nanocups-on-microtubes is mainly in the range of 30 nm to 100 nm. The pore size obtained here is likely to reflect mainly the size of nanocup openings if we consider that the BJH desorption method is based on the assumption that the pores are in cylindrical geometry, and the opening size derived is consistent with the one observed from the TEM image (Fig. 2e). The small opening size further affirms the cup-like morphology described above, putting forward the possibility of utilizing the nanocups as nano-reactors for trapping and synthesis of embedded nanostructures, such as MoS_2 nanosheets. The details about hydrothermal synthesis of MoS_2 nanosheets using the nanocups as the nano-reactors will be elaborated in the next section.

The C-PDA nanocups can also be attached on microspheres instead of microtubes. Through reducing the PS concentration to 15 wt%, the morphology of the electrospinning product could be facilely tuned into microbeads connected by PS nanofibers of a few hundred nanometers in diameter (Fig. $4a_1$ and $4a_2$). Nanopores are also created on the surface of the beads while the

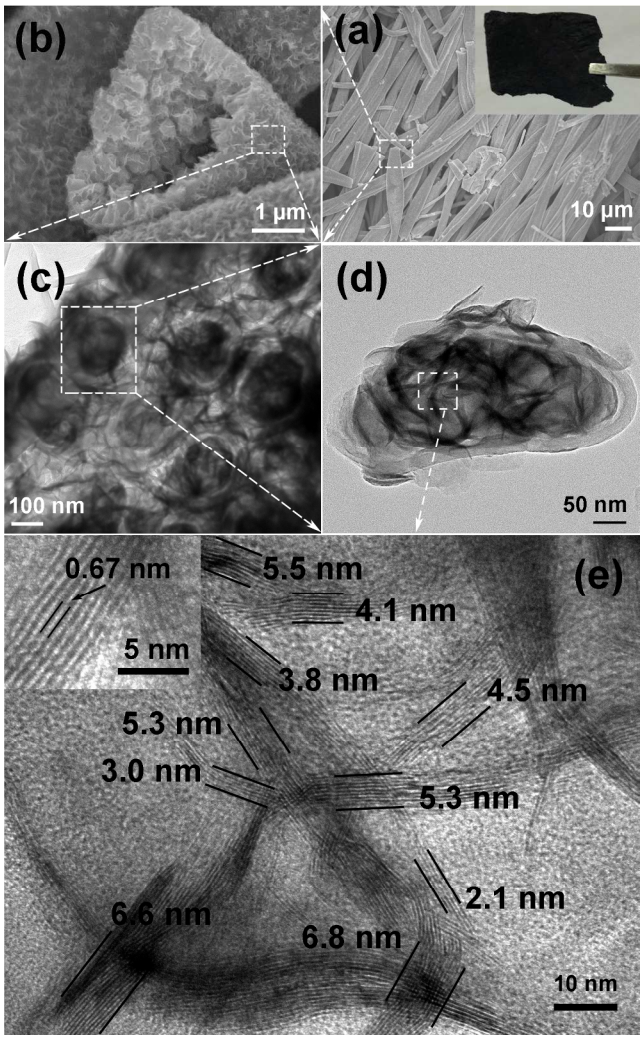

Fig. 5 (a and b) FESEM and (c and d) TEM images of MoS_2 nanosheets constrained in C-PDA nanocups, and inset of (a) shows the free-standing nature of the MoS_2-in-C-PDA nanocups. (e and inset) High-resolution TEM images of formed MoS_2 nanosheets within the nanocups

linker, PS nanofibers, has no pores, indicating that the formation of pores is dependent on the host size. After PDA coating and annealing, hollow microspheres comprised of C-PDA nanocups were also formed (Fig. $4b_1$-$4b_3$). The microspheres are linked by thin hollow C-PDA nanofibers (Fig. $4b_4$).

The preparation of MoS_2-in-C-PDA nanocups and their morphology and structures

As mentioned above, the nanocups-on-microtubes have numerous chambers. The nanocups can be used as host to trap other materials for various applications. As a demonstration, MoS_2 was synthesized within the nanocups using hydrothermal method. Rather than putting the nanocups-on-microtubes in MoS_2 precursor solution during hydrothermal treatment, which would result in uncontrolled growth of MoS_2 within and outside of the structure, a free-standing mat composed of nanocups-on-microtubes was immersed into the precursor solution for a few hours to load the precursors into the nanocups, as demonstrated in the experimental section. After being taken out from the solution, the solution not held in the nanocups will flow away due to the gravity force, ensuring that MoS_2 is mainly formed within the

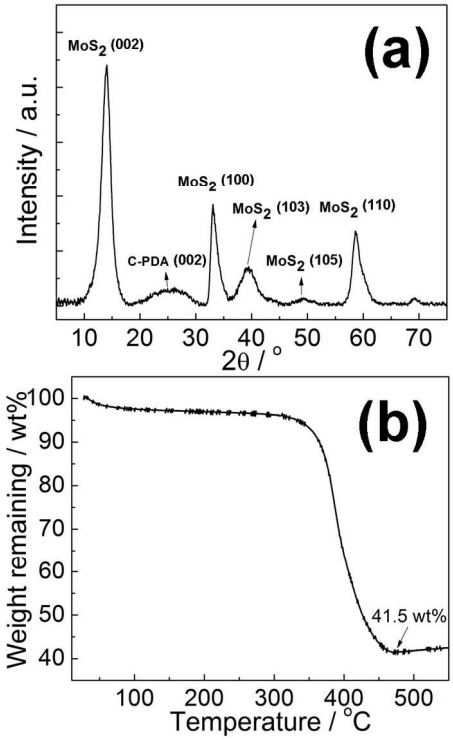

Fig. 6 (a) XRD pattern and (b) TGA curve of MoS_2-in-C-PDA nanocups, confirming the MoS_2 phase and the content of MoS_2, respectively

nanocups. The presence of DI H_2O in the Teflon-lined stainless steel autoclave provides required high pressure for the hydrothermal growth. As shown in Fig. 5a and the inset, uniform and long microtubes in free-standing mat form are retained after the hydrothermal growth. Both the inner and outer surfaces of the microtubes become rougher (Fig. 5b), indicating some MoS_2 precursor solution were adsorbed on the surfaces of the microtubes, which was converted to MoS_2 by the hydrothermal treatment. Despite the small amount of MoS_2 on the surfaces, the TEM images in Fig. 5c and 5d clearly demonstrate that randomly oriented MoS_2 nanosheets with distinct interspaces are mainly trapped within the nanocups, and the edges of most nanosheets are in close contact with C-PDA nanocup inner walls. The high-resolution TEM image in Fig. 5e shows that most of the nanosheets have thickness of less than 6.7 nm. The average inter-planar space is about 0.67 nm for (002) lattice plane (inset of Fig. 5e), indicating that there are maximum 10 layers in each nanosheet. The X-ray diffraction (XRD) pattern of the sample is shown in Fig. 6a. The diffraction peak at $2\theta = 14.1$ ° is from (002) lattice plane of MoS_2. The inter-layer *d* spacing and mean size of the crystalline domains derived from the (002) peak position and full width at half height, respectively, are about 0.64 and 4.2 nm, respectively, again indicating that by average there are only a few layers in each nanosheet. The diffraction peaks at $2\theta = 26.1$ °, 33.2 °, 39.3 °, 49.7 ° and 58.8 ° can be assigned to lattice plane (002) of C-PDA, lattice plane (100), (103), (105) and (110) of MoS_2, respectively, indicating the existence of C-PDA phase as well as the crystalline nature of the MoS_2 nanosheets. The content of MoS_2 is about 46 wt% based on the thermogravimetric analysis (TGA) result (Fig. 6b), taking note that MoS_2 is finally converted to MoO_3 in the TGA measurement in air atmosphere.

The electrochemical properties of the C-PDA nanocups and MoS_2-in-C-PDA nanocups

As introduced above, the C-PDA nanocups have graphitic multilayered structure with a considerable amount of defects and are doped with substantial amounts of pyridinic and pyrrolic N. The electrochemical properties of the neat C-PDA nanocups as a LIB anode were investigated and the results are shown in Fig. 7. Under current rate of 50 mA g^{-1}, the C-PDA nanocups exhibit initial discharge and charge capacities of 1171 and 677 mAh g^{-1}, respectively, with initial coulombic efficiency of 57.8 % (Fig. 7a). The initial irreversible capacity is mainly due to the formation of solid electrolyte interphase (SEI) film on the surface of the C-PDA nanocups that irreversibly consumes extra lithium ions to form lithium organic compounds as well as the irreversible trapping of lithium in the bulk of C-PDA.[40] The formation of SEI film at initial discharge stage is evidenced by the reduction peak at 0.5~0.6 V of the first cyclic voltammetry (CV) curve (Fig. 7b).[41] The galvanostatic discharge/charge profiles of C-PDA nanocups (Fig. 7a) is unlike that of graphite which shows a stable characteristic voltage plateau at low potential of less than 250 mV, indicating that the lithiation/delithiation behaviours of the C-PDA is more than standard stage I formation/extraction of LiC_6 intercalates.[42] This is further confirmed by the CV curves (Fig. 7b), where a slope below 1.0 V on cathodic curve (~1.5 V on the 1st cathodic curve) and a peak that starts at 1.0 V on anodic curve are observed. The overall capacity is mainly resulted from voltage below 1 V (~1.5 V on 1st discharge cycle) during discharge and above 1 V during charge, indicating that the major reaction in the C-PDA anode is metallic lithium plating induced by defects.[40, 43-44] The existence of pyridinic and pyrrolic N also favours reversible lithium adsorption,[41] leading to stabilized reversible capacity of about 550 mAh g^{-1} with coulombic efficiency of almost 100 % after initial few cycles (Fig. 7c). This is higher than the theoretical capacity of graphite, 372 mAh g^{-1}.

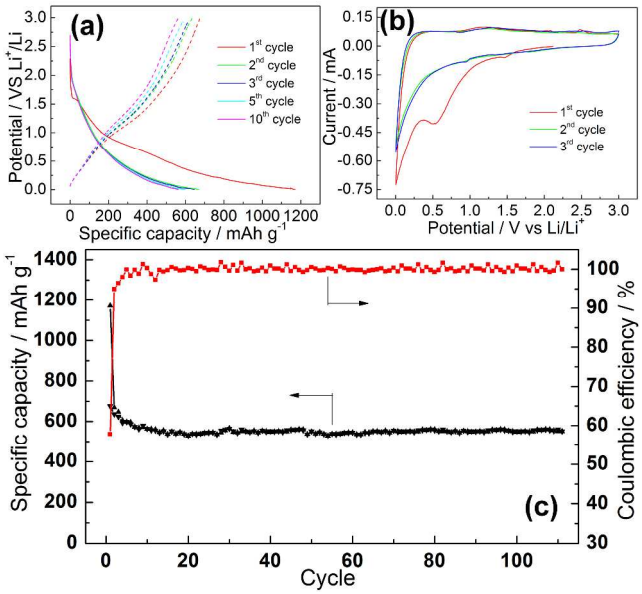

Fig. 7 (a) Galvanostatic discharge/charge profiles (1st, 2nd, 3rd, 5th and 10th cycle), (b) cyclic voltammetry (CV, 1st 2nd and 3rd cycle), and (c) electrochemical performance (cycled capacity and coulombic efficiency) of the C-PDA nanocups as a LIB anode

MoS_2 is a promising material for LIB anodes because its high reversible capacity.[45] In addition, thin MoS_2 nanosheets have large specific surface area and short diffusion length in thickness direction that benefit discharge/charge kinetics. In MoS_2-in-C-PDA nanocups fabricated in this work, the thin MoS_2 nanosheets are uniformly trapped in the C-PDA nanocups, which would allow easy insertion/extraction of lithium ions from the electrolyte in the nanocups, providing a large quantity of accessible reaction sites. The close contact of the nanosheets with the C-PDA nanocups would ensure good electrical conduction. These make MoS_2-in-C-PDA nanocups an attractive candidate for high-rate LIB anodes.

CV curves of MoS_2-in-C-PDA in the first three cycles are shown in Fig. 8a. Typical lithiation/delithiation behaviours for nitrogen-containing carbon and MoS_2 are observed. The weak reduction peak at about 1.4 V on the first cathodic curve is assigned to the reduction of oxygen/nitrogen-containing graphitic carbon (C-PDA),[46] indicating that the C-PDA nanocups are involved in the discharge/charge process. The intensive peaks at about 1.0 and 0.4 V on the first cathodic curve are derived from the intercalation of Li^+ into MoS_2 that forms Li_xMoS_2 (1.0 V) followed by its subsequent decomposition into metallic Mo and Li_2S (0.4 V),[47-49] which are shown as follows:

$$MoS_2 + xLi^+ + xe^- \rightarrow Li_xMoS_2 \quad (1)$$

$$Li_xMoS_2 + (4\text{-}x)Li^+ + (4\text{-}x)e^- \rightarrow 2Li_2S + Mo \quad (2)$$

Noting that the above two cathodic peaks significantly weaken or disappear in the following cycles, showing that the decomposition of Li_xMoS_2 is likely to be irreversible.[45] On the first anodic curve, the shallow peak at about 1.5 V and the intensive one at about 2.3 V are associated with the partial oxidation of Mo that gives MoS_2 and delithiation of Li_2S as shown in the reaction (3) below from right to left direction, respectively.[50]

$$S + 2Li^+ + 2e^- \leftrightarrow Li_2S \quad (3)$$

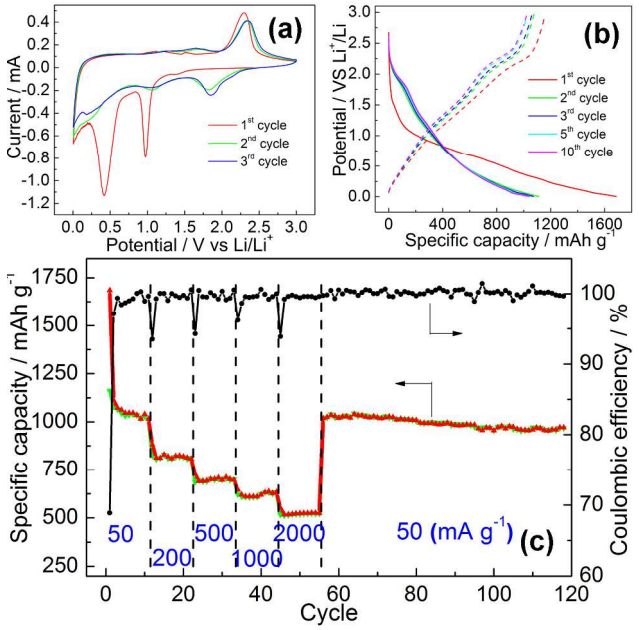

Fig. 8 (a) Cyclic voltammetry (CV, 1st, 2nd and 3rd cycle), (b) galvanostatic discharge/charge profiles (1st, 2nd, 3rd, 5th and 10th cycle) and (c) electrochemical performance of the MoS_2-in-C-PDA nanocups as a LIB anode

In the following cycles, the pronounced cathodic peak at around 1.8 V can be attributed to the lithiation of S as shown in the reaction (3) from left to right direction. The weak peak at about 1.0 V and slop at about 0.2 V can be assigned to the lithiation of the formed MoS_2 (reaction (1)) and the further decomposition of the lithiated MoS_2 (reaction (2)), respectively.[50]

The electrochemical properties, including cycling capacity at the current rate of 50 mA g^{-1} and rate capacity at current rates of up to 2 A g^{-1}, of the MoS_2/C hybrids with about 2 mg in mass are shown in Fig. 8b and 8c. Typical discharge and charge profiles of MoS_2 are observed (Fig. 8b) with initial capacities of around 1685 and 1161 mAh g^{-1}, respectively. The initial coulombic efficiency is about 69 %. Several factors cause the initial irreversible capacity of the nanostructure. Firstly, the irreversible conversion from MoS_2 to Mo in the first discharge cycle consumes excess lithium ions and produces current in the first discharge cycle, giving initial irreversible capacity. Secondly, the initial irreversible capacity of C-PDA nanocups, as discussed above, also partially contributes to the overall initial irreversible capacity. Thirdly, the formation of solid electrolyte interphase (SEI) film at the first discharge cycle consumes extra lithium ions and passivates the surface of the nanostructure,[50-54] trapping part of the alloyed lithium ions. From the second cycle onwards, the capacity is rapidly stabilized at about 1050 mAh g^{-1} with coulombic efficiency of almost 100 %. The fast stabilization is mainly due to the favorable morphology of MoS_2, i.e., it is in the form of randomly oriented thin nanosheets with less than 10 stacked layers, which ensures complete lithiation/delithiation in each cycle. At a current rate of 200 mA g^{-1}, the capacity decreases slightly to around 820 mAh g^{-1}. A high capacity of about 520 mAh g^{-1} can still be delivered at a high current rate of 2 A g^{-1}, demonstrating excellent high-rate performance of MoS_2-in-C-PDA nanocups. The capacity fully rebounds back to about 1000 mAh g^{-1} when the current rate is adjusted back to 50 mA g^{-1}. Good cyclability with coulombic efficiency of above 99 % after the rate test is observed on the same battery cell. Noting that the content of MoS_2 in the nanohybrid is 46 wt%, and hence the normalized capacity of MoS_2 nanosheets is as high as 1524 mAh g^{-1} based on the assumption that the overall capacity is the sum of the capacities of the two components (taking the reversible capacity of the C-PDA nanocups-on-microtubes as about 550 mAh g^{-1}, as shown above). This is close to the highest reported theoretical capacity of MoS_2, about 1675 mAh g^{-1},[45] further verifying that the aforementioned reversible reactions have been utilized to a high extent and also suggesting that extra lithium adsorption at the interfaces of C-S-Mo may occur.

The excellent electrochemical performance of MoS_2-in-C-PDA nanocups can be attributed to the following factors. Compared with those fabricated by deposition of MoS_2 nanostructures on flat surfaces, the trapping of MoS_2 in the C-PDA nanocups gives reasonably high content of MoS_2 as well as close contact between MoS_2 nanosheets conductive C-PDA for good electron transport. The hollow microfibers, the openings of the nanocups and the spaces between neighboring MoS_2 nanosheets also provide effective transport channels for lithium ions. Furthermore, the C-PDA nanocups may act as buffering chamber to effectively accommodate the volume expansion of MoS_2 nanosheets during lithiation/delithiation, leading to excellent structure stability. Therefore, the unique morphology of the C-PDA nanocups-on-microtubes makes it an excellent host to hold active electrode materials for energy storage. The approach may also be extended to other applications where efficient contact between host and guest as well as buffering effect of the host for the guest are crucially required.

Conclusions

Free-standing mats composed of unique C-PDA nanocups attached on hollow microfibers were successfully prepared via self-polymerization of polydopamine on electrospun porous PS microfibers followed by annealing. The nanocups possess diameters and depths of a few hundred nanometers with openings of about 100 nm, and exist as ellipsoid-shaped single cups or interpenetrating twins and triplets. Due to the mechanism of metallic lithium plating that induced by the defectiveness, the pristine multi-layered N-containing carbonaceous nanocups possess reversible capacity of about 550 mAh g^{-1} at 50 mA g^{-1}. The C-PDA nanocups can be used to host active materials for various applications. As a demonstration, thin MoS_2 nanosheets were trapped in the nanocups through controlled hydrothermal growth and the resultant hybrid structure was used as a LIB anode. Good cyclability and excellent rate capacity was achieved owing to the efficient charge transport provided by the good contact of the entrapped MoS_2 nanosheets with the highly conductive nanocups and surrounding electrolyte. The nanocups could also act as buffering chambers to effectively accommodate the volume expansion of MoS_2 during cycling.

Notes and references

[a] *School of Materials Science and Engineering, Nanyang Technological University, 50 Nanyang Avenue, 639798, Singapore; E-mail: asxhlu@ntu.edu.sg*

[b] *School of Mechanical and Aerospace Engineering, Nanyang Technological University, 50 Nanyang Avenue, 639798, Singapore*

† Electronic Supplementary Information (ESI) available: FESEM and TEM images of polydopamine (PDA)-coated PS porous nanofibers. See DOI: 10.1039/b000000x/

# These authors contribut to the work equally

1 W. S. Wang, M. Dahl, Y. D. Yin, *Chem. Mater.* 2013, **25**, 1179.
2 G. L. Li, H. Mohwald, D. G. Shchukin, *Chem. Soc. Rev.* 2013, **42**, 3628.
3 J. B. Joo, M. Dahl, N. Li, F. Zaera, Y. D. Yin, *Energy Environ. Sci.* 2013, **6**, 2082.
4 W. Wei, Z. H. Wang, Z. Liu, Y. Liu, L. He, D. Z. Chen, A. Umar, L. Guo, J. H. Li, *J. Power Sources* 2013, **238**, 376.
5 Z. Jin, F. Wang, J. X. Wang, J. C. Yu, J. F. Wang, *Adv. Funct. Mater.* 2013, **23**, 2137.
6 H. Park, T. Song, H. Han, A. Devadoss, J. Yuh, C. Choi, U. Paik, *Electrochem. Commun.* 2012, **22**, 81.
7 A. La Torre, M. D. Gimenez-Lopez, M. W. Fay, G. A. Rance, W. A. Solomonsz, T. W. Chamberlain, P. D. Brown, A. N. Khlobystov, *ACS Nano* 2012, **6**, 2000.
8 A. La Torre, M. W. Fay, G. A. Rance, M. D. Gimenez-Lopez, W. A. Solomonsz, P. D. Brown, A. N. Khlobystov, *Small* 2012, **8**, 1222.
9 M. D. Gimenez-Lopez, A. La Torre, M. W. Fay, P. D. Brown, A. N. Khlobystov, *Angew. Chem. Int. Ed.* 2013, **52**, 2051.
10 J. Kong, W. A. Yee, Y. Wei, L. Yang, J. M. Ang, S. L. Phua, S. Y. Wong, R. Zhou, Y. Dong, X. Li, X. Lu, *Nanoscale* 2013, **5**, 2967.
11 J. Kong, Y. Wei, L. Yang, W. A. Yee, Y. Dong, R. Zhou, S. Y. Wong, L. Ke, X. W. Sun, H. Du, X. Li, X. Lu, *J. Phys. Chem. C* 2013, **117**, 10106.

12 Y. E. Miao, W. Fan, D. Chen, T. X. Liu, *ACS Appl. Mater. & Interf.* 2013, **5**, 4423.
13 H. Ren, L. Y. Zhang, T. T. Wang, L. Li, Z. M. Su, C. G. Wang, *Chem. Commun.* 2013, **49**, 6036.
14 X. F. Wang, C. Fu, P. Wang, H. G. Yu, J. G. Yu, *Nanotechnol.* 2013, **24**, 165602.
15 S. H. Wu, Y. Hung, C. Y. Mou, *Chem. Mater.* 2013, **25**, 352.
16 D. M. Yang, X. J. Kang, P. A. Ma, Y. L. Dai, Z. Y. Hou, Z. Y. Cheng, C. X. Li, J. Lin, *Biomater.* 2013, **34**, 1601.
17 G. Y. Zheng, Q. F. Zhang, J. J. Cha, Y. Yang, W. Y. Li, Z. W. Seh, Y. Cui, *Nano Letters* 2013, **13**, 1265.
18 O. G. Schramm, M. A. R. Meier, R. Hoogenboom, H. P. van Erp, J. F. Gohy, U. S. Schubert, *Soft Matter* 2009, **5**, 1662.
19 K. S. Iyer, M. Norret, S. J. Dalgarno, J. L. Atwood, C. L. Raston, *Angew. Chem. Int. Ed.* 2008, **47**, 6362.
20 D. G. Shchukin, H. Mohwald, *Adv. Funct. Mater.* 2007, **17**, 1451.
21 J. Fickert, M. Makowski, M. Kappl, K. Landfester, D. Crespy, *Macromolecules* 2012, **45**, 6324.
22 J. Lu, P. Zhang, A. Li, F. Su, T. Wang, Y. Liu, J. Gong, *Chem. Commun.* 2013, **49**, 5817.
23 P. Deotare, J. Kameoka, *J. Nanomater.* 2007, **2007**, 71259.
24 J. He, P. Zhang, J. L. Gong, Z. H. Nie, *Chem. Commun.* 2012, **48**, 7344.
25 D. Jagadeesan, U. Mansoori, P. Mandal, A. Sundaresan, M. Eswaramoorthy, *Angew. Chem. Int. Ed.* 2008, **47**, 7685.
26 H. Jeong, Y. Pak, Y. Hwang, H. Song, K. H. Lee, H. C. Ko, G. Y. Jung, *Small* 2012, **8**, 3757.
27 H. Chun, M. G. Hahm, Y. Homma, R. Meritz, K. Kuramochi, L. Menon, L. Ci, P. M. Ajayan, Y. J. Jung, *ACS Nano* 2009, **3**, 1274.
28 S. Megelski, J. S. Stephens, D. B. Chase, J. F. Rabolt, *Macromolecules* 2002, **35**, 8456.
29 M. Srinivasarao, D. Collings, A. Philips, S. Patel, *Science* 2001, **292**, 79.
30 C. L. Casper, J. S. Stephens, N. G. Tassi, D. B. Chase, J. F. Rabolt, *Macromolecules* 2004, **37**, 573.
31 M. Bognitzki, W. Czado, T. Frese, A. Schaper, M. Hellwig, M. Steinhart, A. Greiner, J. H. Wendorff, *Adv. Mater.* 2001, **13**, 70.
32 J. Kong, W. A. Yee, L. Yang, Y. Wei, S. L. Phua, H. G. Ong, J. M. Ang, X. Li, X. Lu, *Chem. Commun.* 2012, **48**, 10316.
33 L. C. Yang, S. N. Wang, J. J. Mao, J. W. Deng, Q. S. Gao, Y. Tang, O. G. Schmidt, *Adv. Mater.* 2013, **25**, 1180.
34 K. Bindumadhavan, S. K. Srivastava, S. Mahanty, *Chem. Commun.* 2013, **49**, 1823.
35 Y. Gong, S. Yang, L. Zhan, L. Ma, R. Vajtai, P. M. Ajayan, *Adv. Funct. Mater.* 2014, **24**, 125.
36 S. K. Das, R. Mallavajula, N. Jayaprakash, L. A. Archer, *J. Mater. Chem.* 2012, **22**, 12988.
37 Y. F. Zhao, Y. X. Zhang, Z. Y. Yang, Y. M. Yan, K. N. Sun, *Sci. Technol. Adv. Mater.* 2013, **14**, 043501.
38 J. Kong, Z. Liu, Z. Yang, H. R. Tan, S. Xiong, S. Y. Wong, X. Li, X. Lu, *Nanoscale* 2012, **4**, 525.
39 H. Lee, S. M. Dellatore, W. M. Miller, P. B. Messersmith, *Science* 2007, **318**, 426.
40 E. M. Lotfabad, J. Ding, K. Cui, A. Kohandehghan, W. P. Kalisvaart, M. Hazelton, D. Mitlin, *ACS Nano* 2014, 10.1021/nn502045y.
41 X. Wang, Q. Weng, X. Liu, X. Wang, D. M. Tang, W. Tian, C. Zhang, W. Yi, D. Liu, Y. Bando, D. Golberg, *Nano Letters* 2014, **14**, 1164.
42 S. Flandrois, B. Simon, *Carbon* 1999, **37**, 165.
43 R. Mukherjee, A. V. Thomas, D. Datta, E. Singh, J. Li, O. Eksik, V. B. Shenoy, N. Koratkar, *Nat. Commun.,* 2014, **5**, 3710.
44 J. R. Dahn, T. Zheng, Y. Liu, J. S. Xue, *Science* 1995, **270**, 590.
45 T. Stephenson, Z. Li, B. Olsen, D. Mitlin, *Energy Environ. Sci.* 2014, **7**, 209.
46 K. Chang, W. Chen, *J. Mater. Chem.* 2011, **21**, 17175.
47 G. Huang, T. Chen, W. Chen, Z. Wang, K. Chang, L. Ma, F. Huang, D. Chen, J. Y. Lee, *Small* 2013, **9**, 3693-3703.
48 G. Du, Z. Guo, S. Wang, R. Zeng, Z. Chen, H. Liu, *Chem. Commun.* 2010, **46**, 1106.
49 E, Benavente, M. A. Santa Ana, F. Mendizabal, G. Gonzalez, *Coordin. Chem. Rev.* 2002, **224**, 87.
50 X. P. Fang, X. Q. Yu, S. F. Liao, Y. F. Shi, Y. S. Hu, Z. X. Wang, G. D. Stucky, L. Q. Chen, *Micropor. Mesopor. Mater.* 2012, **151**, 418.
51 H. Wang, Z. Xu, Z. Li, K. Cui, J. Ding, A. Kohandehghan, X. Tan, B. Zahiri, B. C. Olsen, C. M. B. Holt, D. Mitlin, *Nano Letters,* 2014, **14**, 1987.
52 A. Ponrouch, P. L. Taberna, P. Simon, M. Rosa Palacin, *Electrochim. Acta,* 2012, **61**, 13.
53 S. Laruelle, S. Grugeon, P. Poizot, M. Dolle, L. Dupont, J. M. Tarascon, *J. Electrochem. Soc.,* 2002, **149**, A627.
54 S. Grugeon, S. Laruelle, L. Dupont, J. M. Tarascon, *Solid State Sci.,* 2003, **5**, 895.